Design of the JHF 200-MeV Proton Linac

Takao Kato
KEK, 1-1 Oho, Tsukuba-shi, Ibaraki-ken, 305-0801, Japan
e-mail: kato@mail.kek.jp

Abstract

A 200-MeV proton linear accelerator for the JHF has been designed [1][2]. A peak current of 30 mA with a 500 μsec pulse duration will be accelerated at a repetition rate of 25 Hz. The designed average current will be 200 μA at the beginning, and nearly 1 mA in the future. The linac consists of a 3-MeV radio-frequency quadrupole linac (RFQ), a 50-MeV drift tube linac (DTL) and a 200-MeV separated-type drift tube linac (SDTL) [3]. A frequency of 324 MHz has been chosen for all of the rf structures. A future upgrade plan of up to 400 MeV is also being considered, in which annular-coupled structures (ACS) of 972 MHz will be used in an energy range of above 150 or 200 MeV. There are three distinct features of the design. The first is stable operation with high performance for a beam-loss problem. The second is a total high shunt impedance, achieved by adopting the SDTL structure. The third is the adoption of klystrons for all of the accelerating structures.

1. Requirements

The required main parameters for the JHF proton linac are listed in Table 1. The construction plan of the linac consists of two stages. An output energy of 200 MeV and a peak current of 30 mA with a pulse length of 500 μsec at a repetition rate of 25 Hz are required in the first stage of construction. The required momentum spread of the output beam is ±0.1%. In order to reduce any beam losses after injection into the ring and to achieve high-intensity operation in the ring, a fast beam chopper in a low-energy region is required. It is crucial for the fast chopping system that the fraction of the particles during the rising and falling times of the chopping pulse be small.

2. Design of the linac

2.1 Design features

The design is summarized in Table 2. A schematic view of the design is shown in Fig. 1. The features of the design are as follows: (1) a frequency of 324 MHz has been chosen for all of the rf structures up to 200 MeV, resulting in no longitudinal transition and suppression of the space-charge effects, (2) an SDTL has been chosen in the energy range from 50 to 200 MeV, resulting in a higher effective shunt impedance, (3) a 3-MeV RFQ has been chosen, resulting in the adoption of quadrupole magnets for the following DTL with sufficient focusing forces, (4) a transition energy of 150 or 200 MeV from the SDTL to the ACS has been

Table 1: Required main parameters of the linac.

	Initial stage	Final stage	
Particles	H^-	H^-	
Output energy	200	400	MeV
Peak current	30	60	mA
Beam width	500	500	μsec
Repetition rate	25	50	Hz
Average current	200	800	μA
Length	< 150	~ 220	m
Momentum spread	±0.1	±0.1	%

selected in the upgrade plan, (5) the equipartitioning focusing method is applied, and (6) the klystrons are used for all of the accelerating structures.

Table 2: Parameters of the JHF 200-MeV proton linac (DTL and SDTL).

	DTL	SDTL	
Frequency	324	324	MHz
Injection energy	3.0	50.1	MeV
Output energy	50.1	200.0	MeV
Length (structure only)	27.0	65.8	m
Length (including drift space)	28.5	92.3	m
Number of tank	3	31	
Number of klystron	3	14	
Rf driving power	3.9	16.7	MW
Total rf power (30 mA)	5.3	21.2	MW
Total length		122.2	m
Total power (30 mA)		26.6	MW
Peak current		30	mA
Beam width		500	μsec
Repetition rate		25	Hz
Average current		200	μA
chopping ratio		~0.56	

2.2 Ion source and RFQ

A promising experimental result (a peak injection current of 13.2 mA with a 90% emittance of 0.55 πmm-mrad was accelerated in the RFQ with a transmission efficiency of 83%) was achieved in the preinjector system (a volume production negative-hydrogen ion source and a 432-MHz RFQ) at KEK [4]. Therefore, a peak current of more than 30 mA from the ion source will be realized if some increases in the transverse emittance are allowed. A four vane-type 324-MHz RFQ has been designed [5]. It accelerates ions from 50 keV to 3 MeV. The detailed design is under development.

2.3 DTL

A 324-MHz DTL accelerates beams from 3 to 50 MeV. It consists of three post-stabilized tanks [6]. An accelerating field of 2.5 MV/m is determined from the viewpoints of satisfying the equipartitioning condition and being sufficiently low for avoiding any discharge problem. All drift tubes contain quadrupole magnets. Model magnets of the holo-conductor type with a magnetic-field gradient of 117 T/m were designed and successfully fabricated [7]. The parameters of the DTL are listed in Table 3.

2.4 SDTL

An SDTL is a new structure concept proposed by the author in 1992 [3]. A 324-MHz SDTL is adopted in medium-energy acceleration from 50 to 200 MeV. Each tank consists of five unit cells. Since the focusing magnets (doublet) are placed between two adjacent SDTL tanks, optimization of the shunt impedance can be easily performed without any geometrical restriction from the quadrupole magnets, which are usually placed in the drift tubes for the DTL system. It is also an advantage from the viewpoint of mechanical engineering that no stabilizing devices are

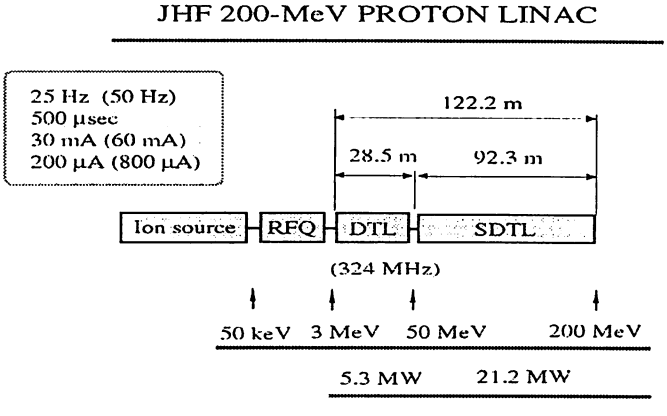

Fig. 1 Schematic view of the JHF 200-MeV proton linear accelerator.

Table 3: Parameters of the DTL

Tank number	1	2	3	
Output energy	19.2	35.4	50.1	MeV
Length	10.4	8.9	7.8	m
Number of cell	80	41	29	
Rf driving power	1.16	1.36	1.40	MW
Total rf power (30 mA)	1.64	1.84	1.84	MW
Accelerating field	2.5	2.7	2.9	MV/m
Stable phase	-30	-26	-26	degree
Bore diameter	13	22	26	mm

Table 4: Parameters of the SDTL

Length of unit tank	1.48 - 2.61	m
Number of tank	31	
Number of cell	155	
Rf driving power	0.35 - 0.64	MW
Total rf power (30 mA)	0.48 - 0.78	MW
Accelerating field	3.86 - 3.6	MV/m
Stable phase	-26	degree
Bore diameter	30	mm

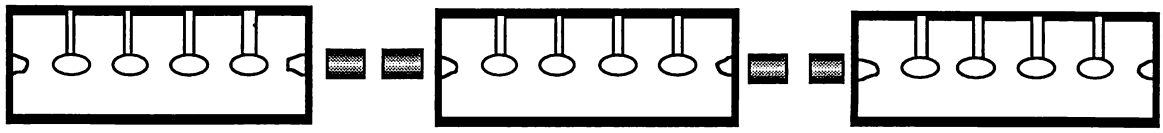

Fig.2 Schematic view of the SDTL structure. Focusing magnets are placed between two adjacent SDTL tanks. Each tank consists of five unit cells.

required in the SDTL system. There are many other advantages in construction due to the simple structure of SDTL: a fewer number of focusing magnets, easier fabrication of the drift tubes, less required accuracy in the alignment of both the drift tubes and tanks. All of the advantages mentioned above result in better cost performance in construction of the medium-energy part of the linac. The parameters of the SDTL are listed in Table 4.

2.5 ACS

An extensive beam-dynamics calculation regarding an upgrade of the output energy up to 400 MeV by using the CCL-type structure was performed [1]. It was concluded that an accelerator complex of DTL, SDL and the annular coupled structure (ACS) is a good choice from the viewpoints of both the output beam quality and the accelerating efficiency. Also, it was pointed out that the ACS is the one which has balanced characteristics of both the shunt impedance and the field symmetry [8]. A frequency of 972 MHz, three-times the fundamental frequency, and a transition energy of above 150 or 200 MeV were selected. The fundamental RF issues concerning the ACS were already solved, and a number of high-power RF tests using the 1296-MHz model cavities were successfully performed [9]. Therefore, a future extension using a 972-MHz ACS will be possible with some modification efforts.

The effective shunt impedance for three kinds of rf structures mentioned above is plotted in Fig. 3.

3. Design features

3.1 Configuration of the linac complex

In proton linear accelerators, the type of accelerating structure changes as the energy increases. The main reason for the change is to optimize the total shunt impedance by changing either the rf frequency or the type of rf structure. A change in the type of accelerating structure,

sometimes associated with a change in the operating frequency, usually causes transitions either in the transverse motion or in the longitudinal one. A transition means an abrupt change in the focusing strength at the transition point, causing a change in the beam motions after the transition. Therefore, it usually results in some additional bad effects upon the beam qualities in comparison with those without any transitions. Therefore, it is important to suppress any additional degradation in the beam properties mentioned above. Within the first construction stage, our design has no longitudinal transition, but a transverse transition by introducing an SDTL structure. Figure 4 shows the configuration of the proton linacs proposed around the world. The positions of both the transverse and longitudinal transitions are indicated in the figure. In the JHF 200-MeV linac design, two transitions are separated by introducing SDTL structures. This type of configuration has some advantages compared with the usually designed (DTL+CCL)-scheme with a multiplied CCL-frequency, as follows:

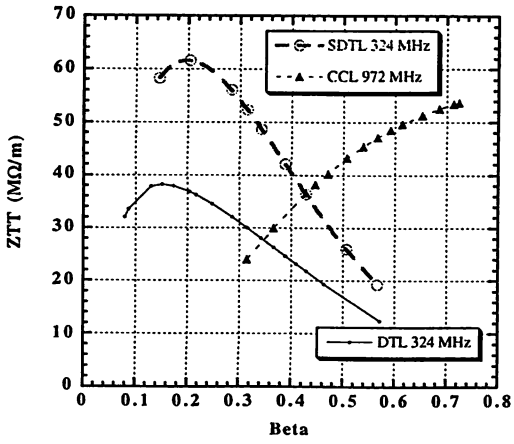

Fig. 3 Effective shunt impedance of the three types of rf structures used in our design.

1) It is normally considered that the rate of phase damping in the CCL is larger than that in the SDTL, because of a difference in the energy-dependence of the transit time factor. Therefore, the volume of a bunch in the SDTL is larger than that in the CCL, assuming the same transition energy from the DTL. Thus, the space-charge effects in the SDTL is weaker than that in the CCL.
2) A longitudinal transition in a linac complex (DTL+SDTL +CCL) occurs at a rather higher energy (150 or 200 MeV). Therefore, in addition to its higher beam energy, the bunch length of the SDTL output beam is sufficiently short, so that the effects of nonlinear problems related to acceleration in the CCL decrease in comparison with a complex involving the DTL and CCL.
3) The number of particles in a bunch is determined by the frequency of the bunching process; it is usually done in RFQ. Therefore, the space-charge effects after a frequency transition seem to be as if the peak current is multiplied by the frequency-transition ratio, compared with the assumed acceleration in which the bunching process begins with the CCL-frequency. Therefore, a large frequency-ratio between the initial rf structure and the final one is not desirable for a high-intensity proton linac.

3.2 Frequency choice

A frequency of 324 MHz is selected for the following reasons:

1) the space-charge effects are greatly reduced compared with a conventional frequency of 200 MHz,
2) the electroquadrupole magnets with a sufficiently strong focusing strength for the drift tubes are possible based on the assumption of a 3-MeV RFQ,
3) a 3-MeV RFQ for a single tank is possible,

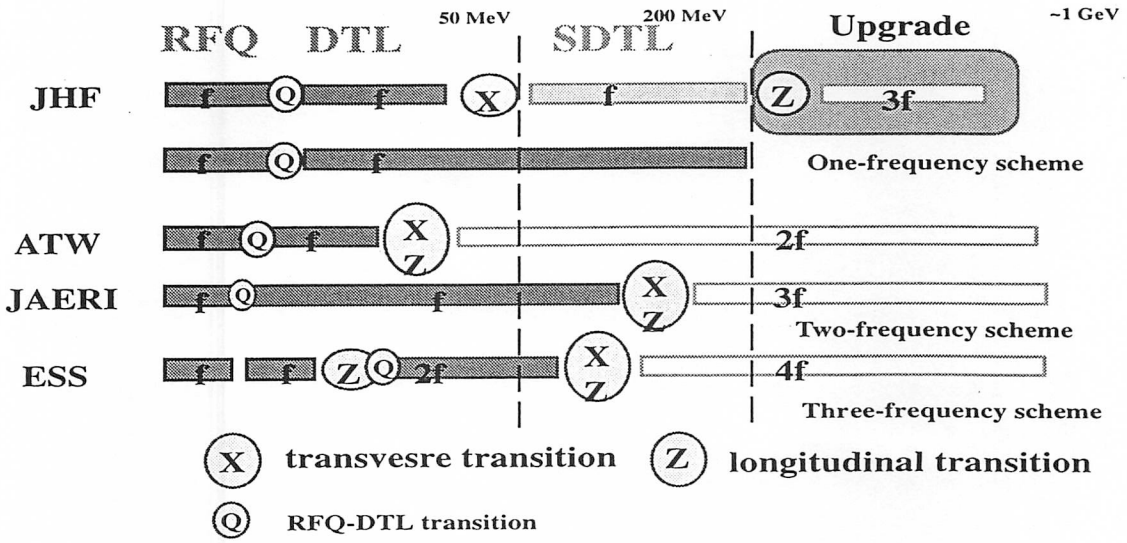

Fig.4 Configuration of the linac; 'f' means the operating frequency.

4) a klystron is possible with some modifications from that at a frequency of 350 MHz, and
5) an ACS for a high-β structure is possible, assuming a frequency multiplication factor of three.

The results of simulation (space-charge strength and emittance growth) from 3 to 148 MeV for two kinds of frequencies (324 and 201 MHz) are given in Table 5. Here, the rms transverse emittance of the injection beam of 0.187 πmm-mrad and the ratio between the transverse emittance and the longitudinal one of 0.5 were assumed based on the assumption that the ion source produces a beam having the same transverse emittance. The peak current was 30 mA. An accelerating field of 2.1 MV/m was used for both simulation based on the assumption that the field strength is determined by the rf power dissipation of the cavity wall, not by a discharge problem. It is noted that the amount of transverse acceptance for both frequencies is equal if the bore radius is determined according to the square-root of the transverse β-function. This means that the ratio of the safety factor (bore size/beam size) is equal for both structures in spite of a large difference in the geometrical size. Judging from the results, it is concluded that a higher frequency is a better choice for a high-intensity, high-energy proton linac, such as the JHF linac. It is also known that the required magnetic-field gradient for the transverse motion is proportional to the square of the frequency and inversely proportional to the particle energy. Therefore, there is a higher limit of frequency, determined by the available focusing design and equipment.

3.3 Focusing design

Both the transverse and longitudinal focusing parameters are determined on the basis of equipartitioning theory combined with coupled envelope equations for the bunched beam (refs. [10-12]). The injection parameters, related to both the beams and structures, are chosen so that the equipartitioning condition is satisfied. The condition is given by

$$\gamma_0 \frac{\varepsilon_{nx}}{\varepsilon_{nz}} \frac{z_m}{a} = 1 \quad \text{or} \quad \frac{k_x \varepsilon_{nx}}{k_z \varepsilon_{nz}} = 1,$$

Table 5: Results of the space-charge effects and the emittance growth in two kinds of simualtions. σ and σ_0 denote the phase advance with and without space-charge effects, respectively. EGF-x/z is the transverse/ longitudinal emittance growth normalized by those for 201 MHz.

	324 MHz	201 MHz
σ_x/σ_{x0}	0.84 - 0.77	0.69 - 0.59
σ_z/σ_{z0}	0.72 - 0.62	0.63 - 0.53
EGF-x	0.66	1
EGF-z	0.51	1

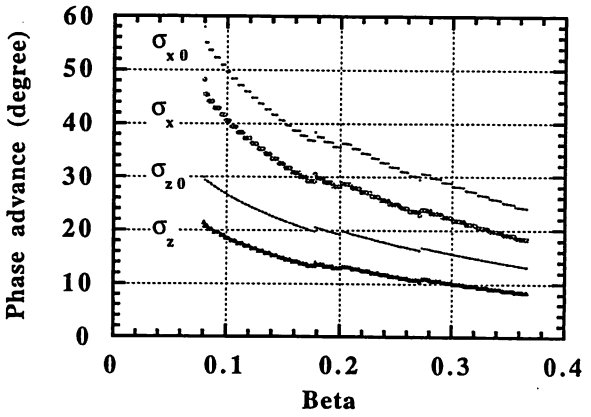

Fig. 5 Phase advances in an equipartitioning focusing scheme for both transverse and longitudinal motions along the DTL. A peak current of 30 mA is assumed.

where suffix n means a normalized emittance and k_x and k_z are the wave numbers of the transverse and longitudinal phase oscillations with space-charge. Figure 5 shows an example of the variation of the phase advances in an equipartitioning focusing scheme for both the transverse and longitudinal motions with a beam current of 30 mA. Figures 6 and 7 show examples of the variation in the rms beam sizes. It can be seen that the bunch shape in the equipartitioning focusing method becomes more spherical as the energy increases.

3.4 Beam simulation for the DTL and the SDTL

Beam simulations were performed using the code LINSAC [13]: the code includes an accurate field distribution in an accelerating gap, and takes account of any space-charge effects by the particle-particle method. It includes all space harmonics into the calculation. Both the emittance growth and halo formation during acceleration were carefully studied, since they are one of the main issues in designing a high-intensity JHF proton linac. The details of the calculated results are given in refs. 1 and 2.

Two sets of normalized rms emittances at the entrance of the DTL were used in the simu-

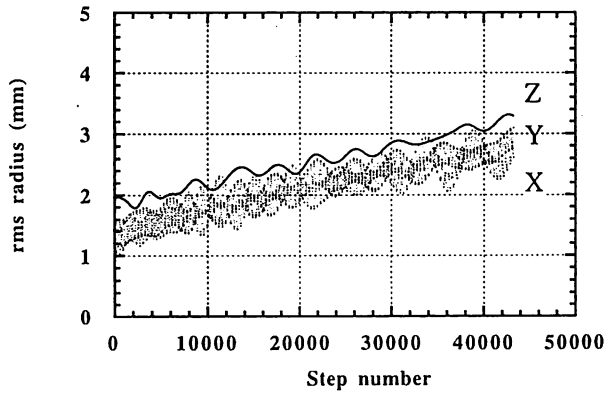

Fig. 6 The rms beam sizes along the DTL from 3 to 148 MeV for the equipartitioning focusing. A unit cell corresponds to 181 calculation steps .

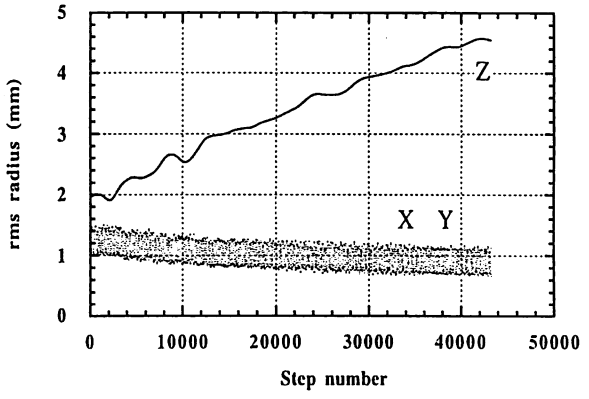

Fig.7 The rms beam sizes along the DTL from 3 to 148 MeV for the constant phase advance (transverse motion) focusing.

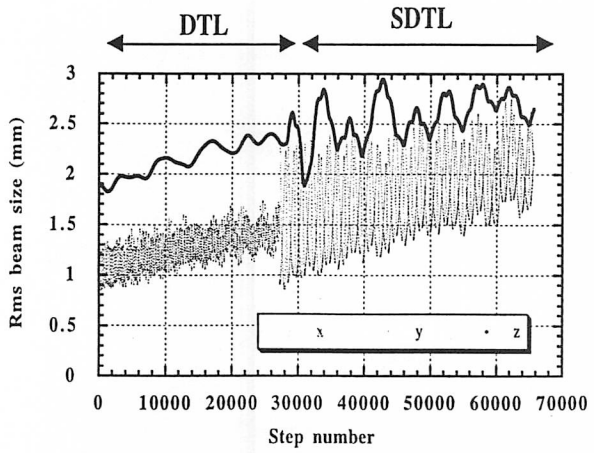

Fig. 8 Calculated rms beam sizes along the linac. A unit cell corresponds to 181 steps. Injection particles of type-B are used. The peak current is 30 mA.

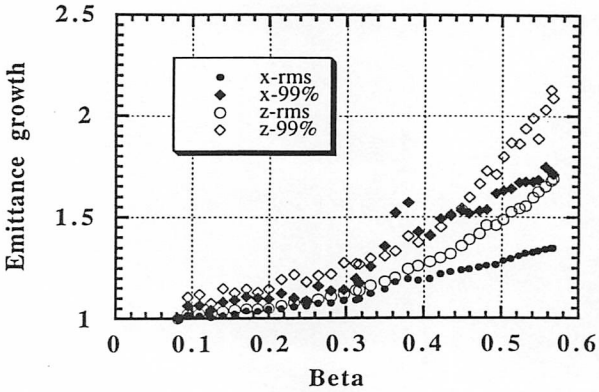

Fig. 9 Emittance growth (rms and 99%) along the linac. A 30-mA type-B injection beam is used.

lation through the DTL and the SDTL (Type A: 0.187 πmm-mrad and 0.133 πMeV-deg and Type B: 0.375 πmm-mrad and 0.266 πMeV-deg). Compared with the transverse-focusing design with a constant phase advance of 60 degrees, the calculated results with the equipartitioning focusing design show better beam qualities totally, especially in both the emittance growth and halo formation in longitudinal phase space [2]. For the type-A beam, the ratios of the emittance growth between two focusing methods (the equipartitioning focusing and the constant phase advance one) are 1.22 and 0.62 in the transverse and longitudinal rms emittances, respectively. Figures 10 and 11 show the output profile at an energy of 148 MeV for all DTL acceleration. It is found that the ratio of halo-like particles is about an order of 10^{-3} ~10^{-4} in a simulation with 48000 particles. The ratios of halo formation between these two focusing methods are nearly equal in the transverse motion and 0.52 in the longitudinal motion. Here, halo-like particles in the transverse motion are defined by those at the outside of 6.5-times the standard deviation of the radial distribution of the output beam, while halo-like particles in the longitudinal motion are defined by those at the outside of 12.5-times the longitudinal output rms emittance.

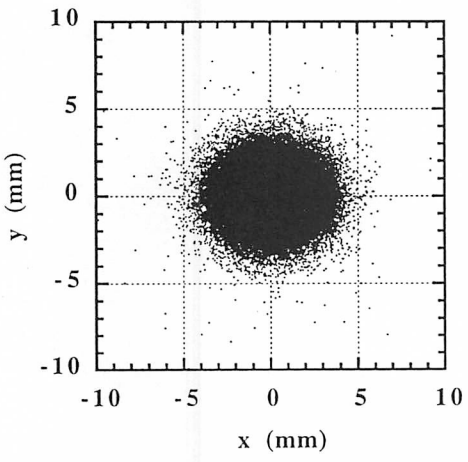

Fig. 10 Output profile of the matched injection simulation. The number of particle is 48000.

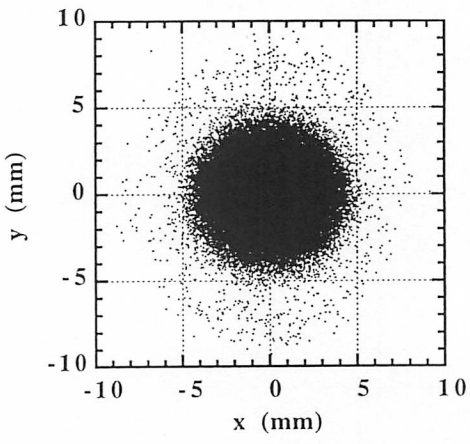

Fig. 11 Output profile of the mismatched injection simulation. The number of particle is 48000.

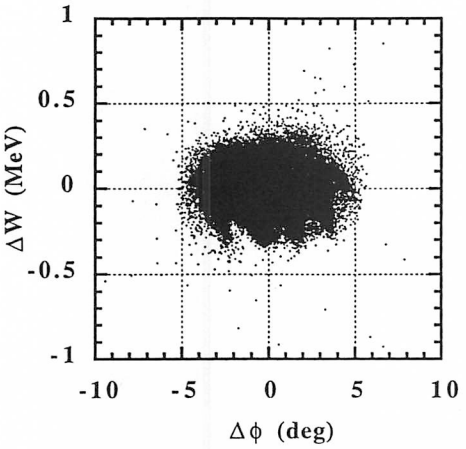

Fig. 13 Longitudinal emittances after acceleration from 3 to 148 MeV for the constant phase advance method. The number of particles is 48000. The beam current is 30 mA.

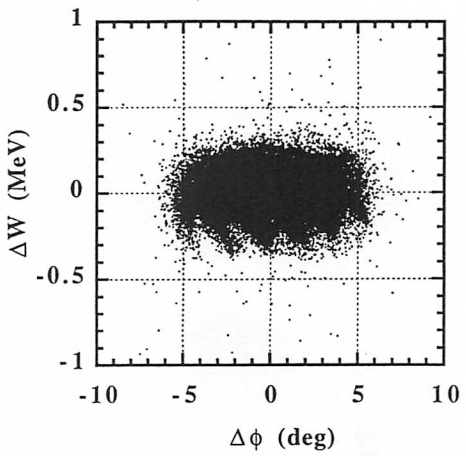

Fig. 14 Longitudinal emittances after acceleration from 3 to 148 MeV for the equipartitioning focusing method. The number of particles is 48000. The beam current is 30 mA.

4. Beam-transport line between the RFQ and the DTL

A beam-transport line, 2.3 m long between the RFQ and the DTL (Fig. 14), has three purposes: achieving both transverse and longitudinal beam-matching, chopping the beam for reducing beam losses after injection into the ring and measuring the beam properties before injection into the DTL [14]. It consists of eight quadrupole magnets, two bunchers and two rf-chopping cavities of a deflecting field of 1.4 MV/m (named RFD) [15] . Figure 15 shows the required micro-pulse structure along with the chopper operation. The beam behavior during transient periods (rising and falling times) is very important from the viewpoint of beam losses during acceleration, since they are deflected by insufficient transverse kicks. There are four micro bunches during the rising time and two during the falling time of the deflecting pulse in the RFD (Fig. 16). It can be seen from Fig. 16 that there are still some live particles during transient periods at the MEBT exit. Figure 17 shows the transmission ratio through the 50-MeV DTL for the micro bunches during the transient periods. Here, three scrapers after each DTL tank were used in order to scrape some fraction of the micro bunches during transient. The scrapers are carefully tuned so as not to have any effects upon the unchopped normal bunches. It can be seen from Fig. 17 that there is no transmitted particles through the DTL when the relative voltage of RFD is larger than 0.5. Figures 18 and 19 show the output emittances for both normal and insufficiently chopped bunches.

It can be concluded from the simulation results mentioned above that high performance in the chopping operation can be achieved in the MEBT and the DTL complex: the number of unstable particles during transient times is less than 0.08% of the total injection particles [16], even in a chopping operation with a rather large loaded Q-value of about twenty. If an equivalent transient time is defined by the fraction of unstable particles during a transient period, the equivalent transient time in the design becomes as small as 0.2 nsec.

5. RF power source

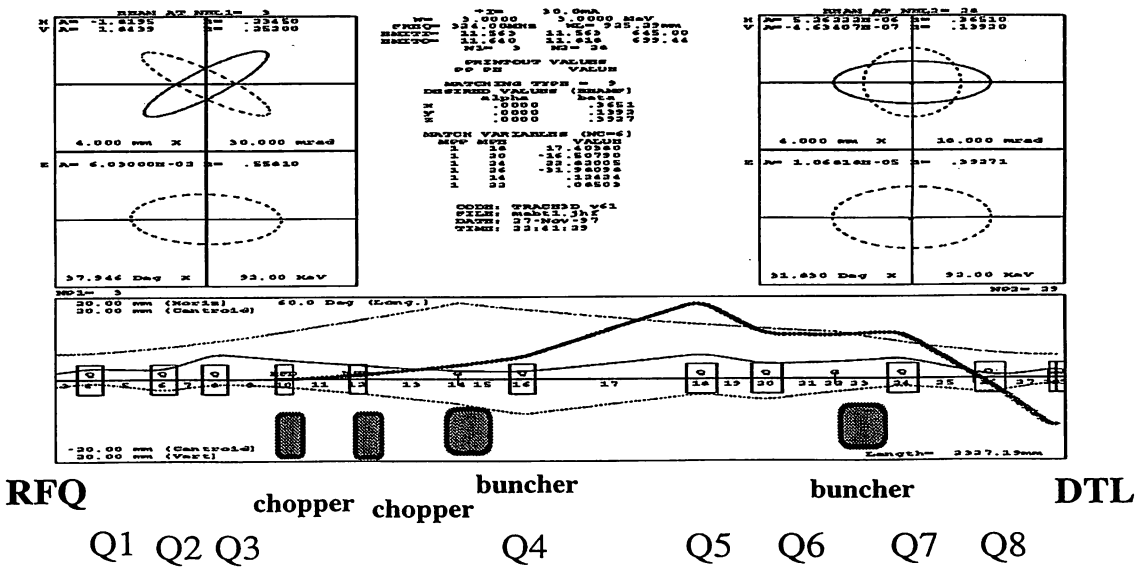

Fig. 14 TRACE 3-D output of the MEBT for a 30-mA type-A beam. The up-left gives the input beam phase spaces and the up-right gives the matched beam with the DTL. The bottom shows the beam profiles in the z, x and y directions, respectively. The dark line traces the beam centroid offset by the two RFDs.

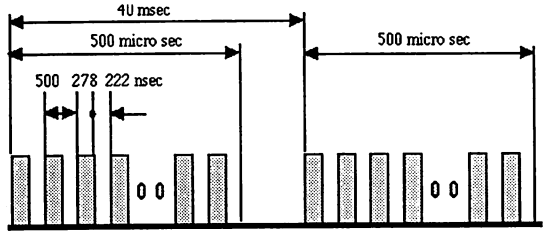

Fig. 15 Required time structure of the beam pulse. A pulse length is 500 μsec. A repetition rate is 25 Hz. The chopping frequency is 2 MHz.

Table 5: Parameters of the RF power source.

Repetition rate	50	Hz
Pulse width	620	μsec
Number of klystrons	19	
Peak output power	2.5	MW

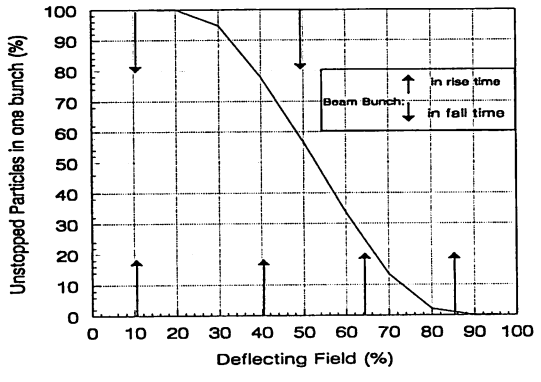

Fig. 16 Unstopped particles ratio in one bunch at the exit of the MEBT vs. the deflecting field level, calculated from PARMILA multiparticle simulations. Arrows stand for every micro bunches during RF rising/falling time.

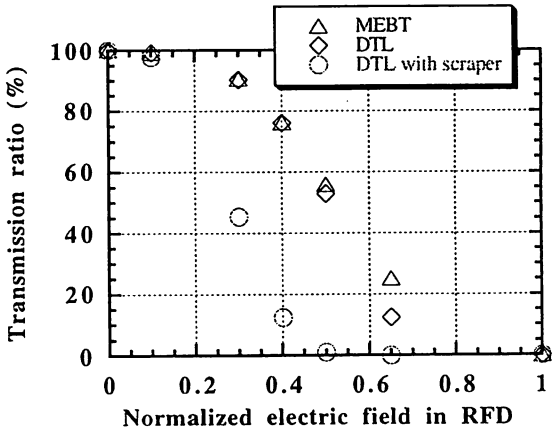

Fig. 17 Transmission ratio through MEBT and DTL vs. RFD field-level during transient periods. Three kinds of transmission ratios are shown: after MEBT, after DTL without the scrapers and after DTL with the scrapers.

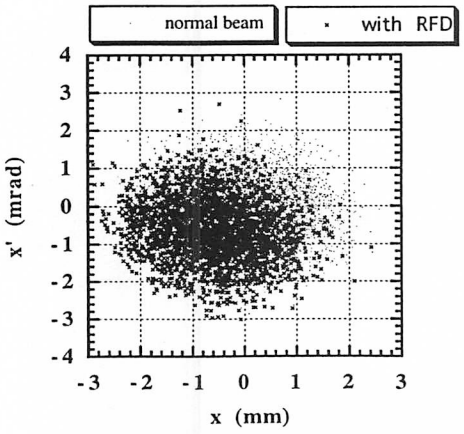

Fig. 18 Output emittances for the normal-unchopped bunch and the chopped one with a 10%-RFD field at the DTL exit. The difference in the emittance shapes is negligibly small.

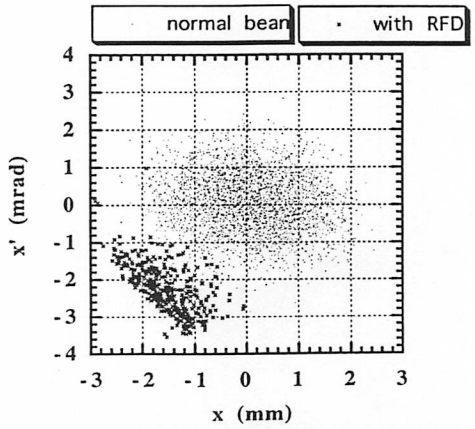

Fig.19 Output emittances for the normal-unchopped bunch and the chopped one with a 40%-RFD field at the DTL exit. Two scrapers after DTL tank-1 and tank-2 are used for eliminating the outer part of the chopped bunch. The ratio of number of particles of the chopped bunch is 12.4% of the normal one.

An RF high-power system has been designed on the basis of accumulated knowledge and experience during construction and operation of the JHP test stand [17]. The main parameters are listed in Table 5.

Acknowledgment

I would like to thank Dr. S. Fu regarding his contribution to the design of the MEBT.

References

[1] T. Kato, 'Design of the JHP 200-MeV Proton Linear Accelerator,' KEK report 96-17 (1997).

[2] T. Kato et al., 'JHF Accelerator Design Study Report, Section 4, 200-MeV Linac,' KEK report 97-16 (1998).

[3] T. Kato, 'Proposal of a Separated-type Proton Drift Tube Linac for a Medium-Energy Structure,' KEK Report 92-10 (1992).

[4] A. Ueno et al., 'Beam Test of the Pre-Injector and the 3-MeV H RFQ with a New Field Stabilization PISL,' Proc. 1996 International Linac Conf., p.293 (1996).

[5] A. Ueno, 'JHF Accelerator Design Study Report, Section 4.4, Preinjector,' KEK report 97-16 (1998).

[6] F. Naito et al., 'Rf Characteristics of a High-Power Model of the 432 MHz DTL,' Proc. 1994 International Linac Conf., p.137 (1992).

[7] K. Yoshino et al., 'JHF Accelerator Design Study Report, Section 4.5, Accelerating structure,' KEK report 97-16 (1998).

[8] Y. Yamazaki, 'Recent Technological Development of Accelerating Structures,' Proc. 1992 Linear Accel. Conf., p.580 (1992).

[9] T. Kageyama et al., 'Development of Annular Coupled Structure,' Proc. 1994 International Linac Conf., p. 248 (1994).

[10] R. A. Jameson, 'Beam-Intensity Limitations in Linear Accelerators,' IEEE Trans. Nucl. Sci. NS-28, 2408 (1981).

[11] R. A. Jameson, 'On Scaling & Optimization of High-intensity Low-beam-loss RF Linacs for Neutron Source Drivers', AIP Conference Proceedings 279 (1993) 969.

[12] M. Reiser, 'Theory and Design of Charged Particle Beams,' Section 5, John Willy & Sons, 1994.

[13] T. Kato, 'Beam Simulation Code Using Accurate Gap Field Distributions in a Drift Tube Linac,' Proc. 1994 International Linac Conf., p.523 (1994).

[14] S. Fu and T. Kato, 'JHF Accelerator Design Study Report, Section 4.3.4, The medium energy beam-transport line,' KEK report 97-16 (1998).

[15] T. Kato, 'New Design of an RF Beam Chopper,' Proc. 7th Symposium on Accelerator Science and Technology, p.288 (1989).

[16] S. Fu and T. Kato, 'Design of Beam-transport Line between the RFQ and the DTL for the JHF 200-MeV Proton Linac,' submitted to APAC'98.

[17] S. Anami et al., 'JHF Accelerator Design Study Report, Section 4.6, RF source,' KEK report 97-16 (1998).